Thermal conductivity and thermodynamics of majoritic garnets: implications for the transition zone

P.A. Giesting [a,1], A.M. Hofmeister [a,*], B. Wopenka [a], G.D. Gwanmesia [b], B.L. Jolliff [a]

[a] *Department of Earth and Planetary Science, Washington University, St. Louis, MO 63130, USA*
[b] *Department of Physics and Pre-engineering, Delaware State University, Dover, DE 19901, USA*

Abstract

Thermal conductivity at room temperature and pressure (k_0), and heat capacity and total entropy as functions of temperature are calculated for majorite–pyrope garnets from new and previous infrared reflectivity and Raman scattering data. The thermodynamic properties, including the effect of cation disorder, vary by less than 4% over this binary, whereas k_0 changes by $>400\%$ due to cation disorder. For mantle garnet compositions (~ 70 mol% majorite), k_0 is ~ 2.3 W/m K, which is $\sim 25\%$ k_0 of ringwoodite, the other major mineral in Earth's transition zone (TZ). The dynamics of the TZ is governed by its two dominant minerals having disparate values for k and viscosity, which parallels the situation in the lower mantle. If the TZ has substantial (60–70%) proportions of majoritic garnet, as suggested by petrological models, then heat flow therein is inhibited relative to the upper and lower mantles. Sub-adiabatic temperatures are implied, which is consistent with steep velocity gradients in the TZ. Association of low thermal conductivity with high temperatures should contribute to the buoyancy of the TZ layer, weaken it, and promote transformation to garnet: such destablization through positive feedback possibly provides a mechanism for catastrophic overturns of the TZ and upper mantle.
© 2003 Elsevier B.V. All rights reserved.

1. Introduction

The flow of heat inside a planetary body is strongly impacted by the thermal conductivity (k) of its constituent phases. The style and mode of mantle convection is the purview of computational geophysics, and for the most part, a constant value of k has been taken to represent the Earth (e.g. [1]). Recent geodynamic studies that allow for the pressure (P) and temperature (T) dependence of k have revealed that many aspects of mantle convection are controlled by the variability of k. For example, boundary layers [2] and plume branching [3] appear different in models

* Corresponding author. Fax: +1-314-935-7361.
 E-mail address: hofmeist@levee.wustl.edu
(A.M. Hofmeister).

[1] Present address: Department of Civil Engineering and Geological Sciences, The University of Notre Dame, Notre Dame, IN 46556, USA.

using variable k as opposed to constant k. Even something as basic as the correlation of the Rayleigh and Nusselt numbers is altered when k departs from a constant [4]. However, pressure and temperature are not the only sources of non-linear behavior of k with depth in the Earth. Layering and heterogeneity also provide dramatic changes in k through compositional effects. Clearly, knowledge of thermal conductivity of the constituent phases of the mantle is needed to make models of mantle convection as realistic as possible. Because d(ln k)/dP occupies a narrow range for dense silicates and oxides [5], knowledge of the thermal conductivity of mantle phases at room temperature and pressure (k_0) is needed to predict k-values at the conditions in the mantle.

Thermal conductivity is difficult to measure directly [6]. The small sizes of high-pressure synthetic samples exacerbate the difficulties; hence, few relevant measurements exist [5]. In particular, k_0 is unavailable for majoritic garnet, which constitutes as much as 60–70% of the transition zone (TZ) of Earth's mantle (e.g. [7,8]). The TZ is a tantalizing region of the Earth, wherein seismic velocities steeply rise, deep earthquakes cease, and some, but not all subducting slabs pass through [9].

This report uses a semi-empirical model [10,11], based on the concepts of a phonon gas and damped harmonic oscillators, to calculate k_0 for majorite–pyrope [Mg$_3$(MgSi)Si$_3$O$_{12}$–Mg$_3$Al$_2$Si$_3$O$_{12}$] solid solutions from new measurements of their vibrational spectra. Closely related properties that are also relevant to the thermal state of the mantle [heat capacity (C_V) and entropy (S_{lat})] are calculated using the quasi-harmonic oscillator model [12,13], and compared to available calorimetric measurements. The effects of Mg–Si ordering and deviations from the cubic garnet structure on the above properties are ascertained. From our calculations and previous results on garnets [11], k_0 is inferred for realistic chemical compositions of mantle garnet, and implications on heat transport in the mantle are discussed.

2. Experimental

Polycrystalline samples with grain sizes of 1–10

μm, in the form of mm-sized disks, were synthesized by hot-pressing in a 2000-ton uniaxial split-sphere apparatus (USSA-2000) at the Stony Brook High Pressure Laboratory [14]. The starting material was very fine-grain powder ground from homogeneous glass of the appropriate composition [15]. Electron microprobe analyses were done using a JEOL-733 using wavelength-dispersive methods [16]. Average compositions in molar percentages are Py$_{100}$, Mj$_{39}$Py$_{61}$, Mj$_{45}$Py$_{55}$, and Mj$_{80}$Py$_{20}$. Indrared (IR) reflectance and thin-film absorption spectra were obtained using a Bomem Fourier Transform IR spectrometer [17]. Dielectric functions were obtained through Kramers–Kronig analyses. Raman spectra from spot sizes of about 1 μm were acquired in the 180° backscattering configuration using a fiber-optically coupled microscope–spectrometer–detector system from Kaiser Optical Systems [18]. For details regarding synthesis, major element chemical compositions, vibrational spectroscopy, and implications for structure and cation disorder of majorite-pyropes, see [18]. This report summarizes the information needed to calculate thermophysical properties. Spectroscopic measurements at higher frequencies (> 1200 cm^{-1}) reveal the presence of OH$^-$, H$_2$O, and various carbonaceous impurities in our samples [19,20], but because the spectral signatures of these impurities are easily distinguished from those of the lattice modes, their presence does not affect our calculations.

3. Vibrational spectra of majorite–pyrope garnets

IR reflectivity (Fig. 1) and thin-film absorbance (Fig. 2) spectra of the Al-rich majorites resemble those of synthetic pyrope, but have extra peaks not expected for a cubic structure. The large number of peaks in Mj$_{80}$ (due to its low symmetry) makes it difficult to recognize the cubic garnet pattern in reflectance (Fig. 1) but absorbance spectra reveal the connections (Fig. 2). Our spectra provide more peaks than do previous measurements of powdered majorites dispersed in KBr [21,22]. Reflectance IR is a quantitative method for single crystals. Two observations show that our reflectivity data obtained from
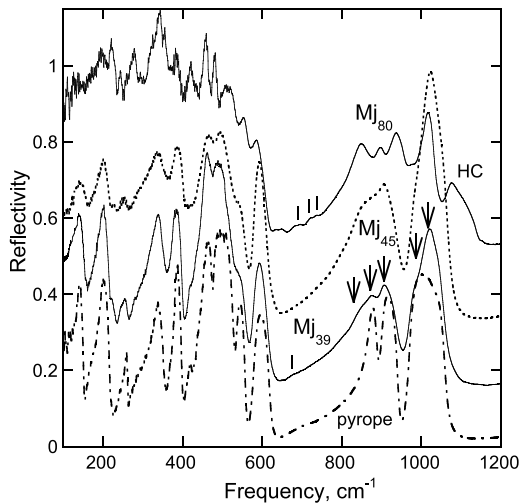
Fig. 1. Raw IR reflectivity spectra of pyrope–majorites, offset for clarity. HC indicates features due to hydrocarbon impurities. Dashed-dotted curve, polycrystalline pyrope; solid, Mj_{39}; dots, Mj_{45}; solid, Mj_{80}. For Mj_{39} and Mj_{80}, the Si–O region has five peaks marked with arrows, rather than the three of cubic garnet. The high reflectivity values for Mj_{80} below 400 cm^{-1} are due to back-reflections for the fine grain sizes of this sample [18]. Extra peaks in the Si–O–Si bending region (local modes, see text) are marked by tics (see text). HC, hydrocarbons.

polycrystalline samples are accurate: (1) polycrystalline pyrope provides virtually the same reflectivity as natural, end-member pyrope [23], and (2) the optical functions calculated from our reflectivity data agree well with our absorption measurements [18].

The Raman spectrum of polycrystalline pyrope (Fig. 3) closely mimics previous measurements of natural, nearly end-member pyrope (e.g. [13]). The Raman spectrum of Mj_{45} closely resembles those of other mid-binary samples [22,24]. The broad peak widths for majorites near the binary mid-point indicate that these compositions are disordered. Spectra of our Mj_{80} resemble Mj_{93} and Mj_{100} examined by Rauch et al. [25], but not Mj_{80} of Manghnani et al. [24], which appears to be almost completely disordered [26]. Our Mj_{39} sample is inhomogeneous on a micrometer scale, ranging from Mj_{26} to Mj_{45}. The average composition is appropriate for the IR measurements because large areas are sampled with this technique. However, the particular spot examined by Raman spectroscopy is more aluminous than Mj_{39}, as in-
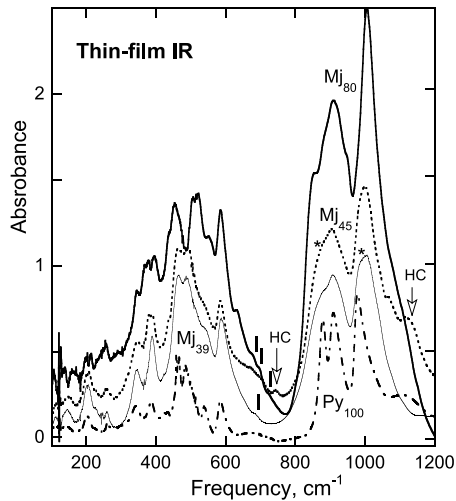

Fig. 2. IR absorption spectra of thin films, calculated from transmitted intensity using natural logarithms. Line types and symbols as in Fig. 1, except that asterisks indicate weak peaks [18]. Sample thickess is ~1 μm for Mj_{80}, ranging to ~0.2 μm for pyrope.

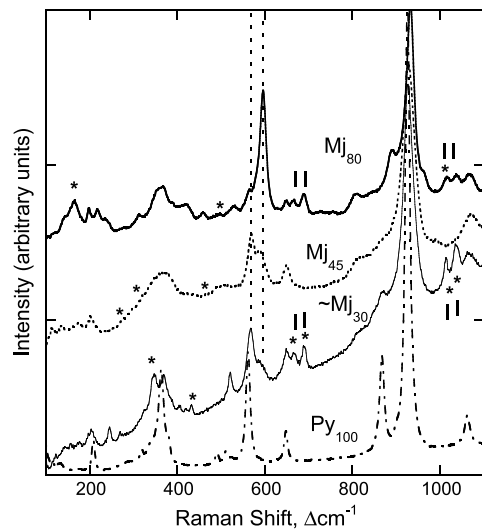Fig. 3. Unpolarized (scrambled) Raman spectra of pyrope–majorites, offset for clarity, but uncorrected for background. Symbols as in Figs. 1 and 2. Peaks that are strongly polarized are indicated by asterisks (some of these were not resolved in scrambled measurements shown here). Dotted vertical lines indicate positions of the two tracer peaks for Mj and Py contents, at 600 and 560 Δcm^{-1}, respectively.

dicated by the narrow peak widths, the specific peak positions, and the relative intensities of the peaks at 560 and 600 Δcm^{-1} (Fig. 3). Most likely, the composition probed by Raman spectroscopy is near Mj_{30} [18].

Raman and IR peak parameters obtained from fits to pure Lorentzian shapes are described in detail by Hofmeister et al. [18]. Theoretical underpinnings for our approach are in Hofmeister [10] and Giesting and Hofmeister [11]. Only the spectral data needed to calculate thermal conductivity, heat capacity, and entropy are presented here.

Peaks not expected for cubic garnet are seen for all majorites in the Si–O stretching region, and for the Al-poor majorites throughout the spectra. A detailed analysis of the changes across the binary of both IR and Raman data and the response of the Raman peaks to polarization confirms that the tetragonal $I4_1/acd$ space group deduced by Nakatsuka et al. [27] is present from $\sim Mj_{30}$ to $\sim Mj_{80}$ [18]. Near the majorite end-member, the space group is $I4_1/a$ (e.g. [28]). As discussed below, the calculations of C_V, S, and k_0 are not impacted by the particular space group, whereas ordering is relevant.

Extra (local) modes are known to occur in solid solution series due to changes in mass or in bonding [29]. The appearance of extra peaks in the Si–O–Si bending region between 650 and 750 cm^{-1} for some compositions in Figs. 1–3 results from such an effect. The associated occurrence of extra peaks near 1000 cm^{-1} and the limitation of such effects to compositions near $\sim Mj_{30}$, Mj_{80} (Fig. 3), Mj_{93}, and to some samples of Mj_{100} (e.g. [25]) suggests that the extra peaks result from cation disorder. Hofmeister et al. [18] deduced that the Si tetrahedron in majoritic garnets does not always vibrate as if isolated, as is the case for garnets without octahedrally coordinated Si. The symmetric bend and stretch of the tetrahedron are altered to a Si_{oct}–O–Si_{tet} bend and a Si_{oct}–Si_{tet} stretch. This behavior is not seen near Mj_{50} as each tetrahedron (on average) is corner-linked to the same species in the surrounding octahedra (1Mg, 1Si, and 2Al), and thus local imbalances in bonding are mitigated by averaging over a slightly greater distance than next-nearest neighbors. Similarly, modes originating in coupled vibrations of octahedra and tetrahedra should not exist in fully ordered majorite. But $MgSiO_3$ majorite commonly is partially disordered (e.g. [30,26]), and such samples possess these peaks. The maximum number of Si_{oct}–O–Si_{tet} vibrations is expected near Mj_{25} and Mj_{75}. At these compositions, about half of the tetrahedra are affected.

4. Heat capacity and entropy

4.1. The quasi-harmonic oscillator model

In Kieffer's [12] model, heat capacity at constant volume (C_V) is calculated by summing the energies contributed by all of the vibrational modes in the solid. We use symmetry analysis and band assignments to construct a density of states (e.g. [13]). Our approach does not utilize any fitting parameters (see discussion in [17]). To compare the model to calorimetric determinations, the thermodynamic relationship is required:

$$C_P = C_V + TV\alpha^2 K_T \tag{1}$$

where α is the thermal expansivity and K_T is the isothermal bulk modulus. For pyrope and grossular, the Kieffer approach is accurate to $\pm 1\%$, largely due to the smoothing process inherent in summing many modes [13]. The lattice contribution to the entropy is obtained from:

$$S(T) = \int_0^T (C_P/T')dT' \tag{2}$$

Cation disorder provides an additional configurational contribution to S. Under the high temperatures expected in the mantle, disorder should prevail, destablizing the ordered $I4_1/a$ structure for majorite–pyropes [31]. Because the transition between cubic garnet and the tetragonal $I4_1/acd$ structure is driven by electrostatic forces, rather than by ordering [27], it is not clear which of these two space groups is stable in the mantle. However, as both structures have only one octahedral site, only the Al–Si disorder on this site need be considered. From Ulbrich and Waldbaum [32]:

$$S_{conf,mj-py} = -R[x\ln(x/2) + (1-x)\ln(1-x)] \tag{3}$$

where $R = 8.314$ J/mol K is the gas constant, x is

the Mj fraction, and Al and Si are presumed to be the only cations in the octahedral site. The possible minor amounts of Cr and Ti on this site are not considered. Configurational entropy will also arise from the substitution of Fe^{2+}, Ca^{2+}, or Mn^{2+} for Mg^{2+} in the dodecahedral site. This contribution to the entropy is also neglected for simplicity, but it can be deduced for the various possible compositions and structures [32].

The quasi-harmonic model [12] is adopted. Some authors [33] have tried to address anharmonic behavior by including the temperature dependence of the vibrational frequencies. However, the latter approach is neither consistent with the partition function used to derive the mode heat capacities nor does it include all the necessary correction terms [34].

4.2. Calculations of heat capacity and comparison with calorimetry

The density of states for pyrope [13] is appropriate for the majorite garnets that do not have Si_{oct}–O–Si_{tet} bending and Si_{oct}–Si_{tet} stretching modes (i.e. octahedral–tetrahedral coupling), as both tetragonal structures ($I4_1/a$ or $I4_1/acd$) have the same total number of modes and the same mode types as does cubic garnet. The changes in space group convert inactive modes into those stimulated by Raman or IR techniques [18,22]. The previously used density of states [13] was modified slightly (Model 1 in Table 1) to account for recent measurements of pyrope [35] and to regroup the Si–O stretching frequencies so that the highest frequency E_g mode, which is clearly

Table 1
Density of states models for the optic modes and heat capacity calculations and measurements for the pyrope–majorite binary

Type	Modes	No.	Input ν (cm^{-1})			
			Pyrope	Mj$_{45}$	Mj$_{80}$	Mj$_{100}$[a]
Model 1: Isolated tetrahedral vibrations						
Einstein	Raman ν_3	6	1062	1070	1068	1065
Einstein	IR ν_3	6	972	988	977	970
Einstein	$\nu_1 + E_g\nu_3$	12+4[b]	926	929	933	930
Einstein	ν_3	20[b]	900	892	890	885
Continuum	ν_4	36	650–512	650–514	649–510	647–516
Continuum	ν_2	24	562–437	569–437	569–421	554–428
Continuum	R	36	383–337	380–333	374–332	380–334
Continuum	T(oct.)	24	478–259	476–255	473–259	480–259
Continuum	T(Mg)	36	271–195	277–203	280–199	273–196
Continuum	T(SiO$_4$)	33	342–131	350–136	355–136	355–136
C_V at 298 K (J/mol-K)			326.6	326.4	326.8	326.9
Model 2: Coupled tetrahedral–octahedral vibrations						
Continuum	Si_{oct}–Si_{tet}	6[b]	n.a.	n.a.	1038–1014	varies
Continuum	Si_{oct}–O–Si_{tet}	12[b]	n.a.	n.a.	722–666	varies
C_V at 298 K (J/mol-K)			n.a.	n.a.	320.8	varies
Calorimetric measurements						
C_P at 298 K (J/mol-K)			325.3[c]	–	–	317[d]

ν_1, symmetric stretching; ν_2, symmetric bending; ν_3, asymmetric stretching; and ν_4, asymmetric bending. R, rotation/libration, all of the SiO_4 tetrahedron; T, translation; n.a., not applicable.

[a] Rauch et al. [25].

[b] Model 2 uses the same parameters as Model 1, except that the ν_1 and ν_2 categories of Model 1 are reduced by six and 12 modes, respectively, and are replaced by the coupled octahedral–tetratrahedral modes listed under Model 2.

[c] Adiabatic calorimetry of Haselton and Westrum [36], accuracy is $\sim 0.5\%$.

[d] Differential scanning calorimetry of Yusa et al. [37] for majorite with $\sim 15\%$ Mg–Si disorder, accuracy is $\sim 2\%$. Comparison of enstatite C_P measured by these authors to adiabatic calorimetry of Krupka et al. [38] suggests that the true value for majorite could be 319.8 J/mol K.

observed only in pyrope, is not used as an input parameter. Model 1 assumes that no coupling of tetrahedral and octahedral Si exists. A second density of states (Model 2 in Table 1) was constructed by including the 'extra' Si_{oct}–O–Si_{tet} bending and Si_{oct}–Si_{tet} stretching modes as separate categories, and by assuming that the maximum amount of coupling occurs. Our assumption of maximum disorder is appropriate for the mantle, because compositions near Mj_{75} are expected [7].

Calculated C_V values are independent of composition, assuming that the mode types of cubic garnet exist across the binary (Table 1). The thermodynamic adjustment between C_P and C_V (Eq. 1) is 3.6 J/mol K at 298 K for pyrope [13], and is nearly constant across the series, as α, V, and K_T do not change significantly (see Table 2 legend). Because of the insensitivity of the calculations to composition, comparisons to measurements of the end-members will be used to establish C_P for the binary, with consideration given to the possible presence of octahedral–tetrahedral coupling.

Calculated C_V values are close to C_P measurements of pyrope [36]. The difference between calculated C_V and measured C_P is 3.6 J/mol K

(1.5%), which is comparable to the uncertainty of the calculation itself. Therefore, for fully ordered majorite, and compositions near Mj_{50}, one would also expect the measurements of C_P to be near C_V. Yusa et al.'s [37] measurement of C_P of 317 J/mol K for Mj_{100} is lower by 10 J/mol K, but exactly equals the predicted C_V of Mj_{80} when the Si_{oct}–O–Si_{tet} modes are included. Note that Yusa et al. [37] also measured the enstatite polymorph, obtaining 81.3 J/mol K, which is slightly lower than the previous C_P of 82.06 J/mol K [38]. Because the adiabatic method used by Krupka et al. [38] is accurate to 1/2% or better, the values of Yusa et al. [37] are low by about 0.7 J/mol K for enstatite, suggesting that the majorite values could be low by the same percentage, which comes to 2.8 J/mol K for garnet. When C_P of Yusa et al. [37] is adjusted for this instrumental error, it matches the calculation for garnets with octahedral–tetrahedral coupling. However, it is possible that such a correction is not needed, and that the occurrence of a larger mismatch between the calculations and measurements for majorite than was observed for pyrope is due to other factors. The cause cannot be greater disorder (i.e. consequently higher amounts of tetrahedral–octahedral cou-

Table 2
Calculated thermal conductivity and relevant physical parameters at room temperature for the majorite–pyrope binary

Sample	k_0	$\langle FWHM \rangle$		C_V	Entropy	
	W/m K	cm^{-1}		J/mol K	$S_{lattice}$	S_{config}
		Reflectance	Raman		J/mol K	J/mol K
Mj_{100}	9.77	–	5[a]	314[b]	260	5.76
$Mj_{93}Py_7$	4.48	–	11[a]	316	261	7.47
$Mj_{80}Py_{20}$	2.74	18.1	21	317	262	8.77
$Mj_{45}Py_{55}$	2.41	21.3	29	322	266	8.34
$Mj_{39}Py_{61}$[c]	2.62	19.4	–	319	264	7.81
Mj_{30}[c]	3.49	–	14.5	317	262	6.81
Py_{100}	5.40	10.3	10.9	322[d]	266[d]	0
Natural Py[e]	5.55[f]	9.4[f]	11.4	322[d]	266[d]	0

FWHM from Hofmeister et al. [18] except as noted. See text for a discussion of heat capacity and entropy. Linear interpolations were used between M of 403.13 g/mol for Py and 401.55 g/mol for Mj; ρ of 3.58 g/cm^3 for Py and 3.56 g/cm^3 for Mj; u_P of 9.10 km/s for Py and of 8.90 km/s for Mj; u_S of 5.08 km/s for Py and of 5.00 km/s for Mj ([15] and references therein).
[a] Typical FWHM from Rauch et al. [25].
[b] Eq. 1 applied to C_P of majorite with 10–20% disorder from Yusa et al. [37].
[c] The Mj_{39} sample is inhomogeneous. IR data represent the average composition (Mj_{39}), whereas Raman data were acquired from an Al-rich spot ($\sim Mj_{30}$).
[d] Eq. 1 applied to C_P of Haselton and Westrum [36]. See text for solid solutions.
[e] Single-crystal natural pyrope from Dora Maira with 94 at% Mg, 4% Fe, 2% Ca; sample number GTF3 in [23].
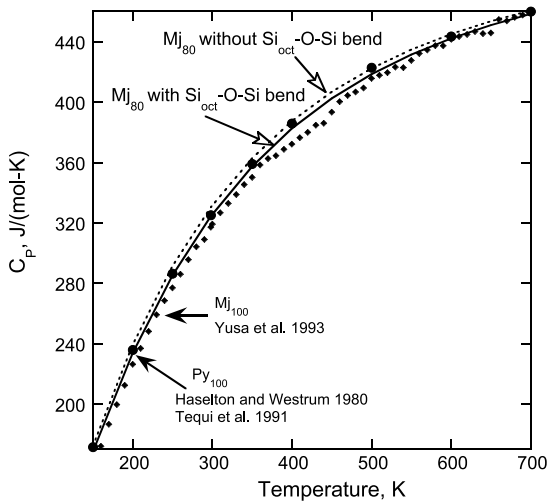[f] Giesting and Hofmeister [11].

Fig. 4. Heat capacity vs. temperature over the same temperature range as calorimetric measurements of majorite. Diamonds, data of Yusa et al. [37]. Calculations for Mj_{100} are indistinguishable for the curves shown for Mj_{80}. Large dots, adiabatic calorimetric data for pyrope by Haselton and Westrum [36], obtained below 350 K or by Tequi et al. [40] for $T > 350$ K.

pling), because the calculation assumed the maximum coupling. The discrepancy might arise from changes in bonding due to the presence of OH^- impurities, which commonly occur in high-pressure synthesis products and specifically in majorites [19,39]. For simplicity, we assume that the C_P value for end-member majorite of Yusa et al. [37] is correct. For Mj contents of $\sim 25\%$ and $\sim 75\%$, C_P of 320 J/mol K is derived from the vibrational calculations with coupled modes. Near Mj_{50}, the measured C_P of pyrope of 326 J/mol K [36] holds. Heat capacity for compositions between the above values are obtained by interpolation, and C_V in Table 2 is deduced by subtracting 3.6 J/mol K from C_P.

Calculated and experimental curves for heat capacity of majorite–pyropes all converge at both limiting temperatures (150 and 700 K) for the Mj_{100} measurements (Fig. 4). The curves never differ by more than a few percent within that range. Below 150 K and above 700 K, the calculated heat capacities with and without the presence of octahedral–tetrahedral coupling merge (data not shown). Below 150 K, all calculations and the measured C_P of pyrope are indistinguish-

able. We conclude that pyrope values for C_P should be used for majoritic garnets at temperatures either below 150 K or above 700 K. Tequi et al. [40] provide a parameterization for pyrope that can be extrapolated to very high temperatures possible in the mantle, repeated here for convenience:

$$C_P(T) = -592.635 + 138.003\ln(T) + 191.204 \times 10^3/T -$$

$$72.066 \times 10^6/T^2 + 79.749 \times 10^8/T^3 \qquad (4)$$

4.3. Calculation of entropy for the majorite–pyrope binary

The lattice contribution to S at 298 K in Table 2 is obtained by integration over the measured C_P of pyrope up to 150 K in Eq. 2, and by use of the compositional dependence for C_P described above for $T > 150$ K. The results depend weakly on Mj content, and the differences are overshadowed by the configurational entropy obtained from Eq. 3 (Table 2). The total entropy (obtained by summing the last two columns in Table 2) depends non-linearly on composition, but reaches a max-
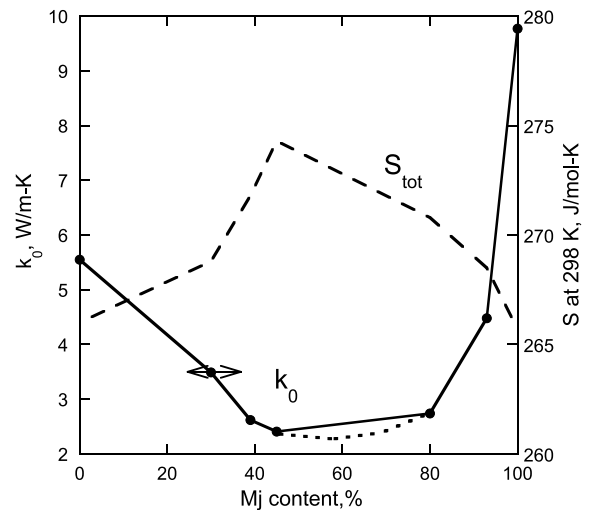

Fig. 5. Thermal conductivity (solid line) and total entropy (dashed line), both at 298 K, across the majorite–pyrope binary. The double arrow indicates the ranges in composition possible for the Raman measurement of the inhomogeneous Mj_{39} sample. Dotted line is an estimate for k_0 near the middle of the binary.

imum near the mid-point of the binary, with essentially equal values for the end-members (Fig. 5).

5. Thermal conductivity

5.1. The phonon gas-damped harmonic oscillator model

By equating phonon scattering to molecular collisions, Debye developed a simple formula for the thermal conductivity of an insulator by analogy to the kinetic theory of gases. Subsequent researchers focused on acoustic modes and approximated the phonon lifetimes in various ways from Grüneisen parameters (summarized in [41]). The accuracy was disappointing. The recognition that phonon lifetimes obtained from vibrational spectra (e.g. from Kramers–Kronig analysis [42]) pertain to heat transfer provided pressure derivatives of k that are as accurate as available measurements [5]. Subsequent refinements to the model [10,11] have shown that the calculation at room temperature and pressure is as accurate as the best conventional measurements ($\pm 5\%$) for mineral structures found in the mantle, and that the model is valid for end-member compositions as well as solid solutions. The calculation uses no free or fitting parameters. For cubic garnets, the formula is:

$$k_0 =$$
$$[\rho/(3ZM)]\ C_V[(u_P + 2u_S)/3]^2/(2\pi\langle \mathrm{FWHM}\rangle) \quad (5)$$

where ρ is density; Z is the number of formula units per primitive unit cell; M is the mass of the formula unit; u_P and u_S are the compressional and shear sound speeds; and $\langle \mathrm{FWHM}\rangle$ is the averaged full width at half maximum (in wavenumbers) of peaks in the Raman spectra and/or in the imaginary part of the dielectric function (ε_2) derived from IR reflectivity. Because all known structural varieties of 'garnet' have four formula units in the primitive cell (e.g. [27]), Eq. 5 should be valid for majoritic garnets.

5.2. Calculations of k_0

Most of the parameters in Eq. 5 change linearly across the series (see legend in Table 2), and their variation from pyrope to majorite is small. The only exception is the average FWHM, which is low for the end-members, increasing towards the middle of the binary (Table 2). The FWHM of majorite is considerably smaller than that of pyrope, according to the Raman measurements of Rauch et al. [25]. Peak widths are similarly asymmetric across the pyrope–almandine (($Mg,Fe)_3$-$Al_2Si_3O_{12}$) and grossular–andradite ($Ca_3(Al,Fe)_2$-Si_3O_{12}) binaries [11]. In calculating k_0, we used the IR reflectivity data, when available, which give a lower FWHM, and thus an upper limit for k_0. Uncertainties are between $\pm 5\%$ and $\pm 10\%$ for k_0 (Table 2).

5.3. Comparison with known behavior of garnet solid solutions

The resulting variation of k_0 across the majorite–pyrope binary (Fig. 5), including the much higher values for the end-members, the asymmetric dependence on composition, and the flat region near the mid-point, reproduces the behavior seen previously for other garnets. Both direct measurements and spectroscopic modeling of k_0 for pyrope–almandine and grossular–andradite binaries exhibit this behavior [11]. Experimental determinations of k_0 from yttrium aluminum–ytterbium aluminum synthetic garnets are also asymmetric [43].

The minimum in k_0 is estimated to be 2.2–2.3 W/m K for Mj_{50} to Mj_{60}, which is lower, but comparable to the minimum of 3.25 W/m K for pyrope–almandine garnets and of 3 W/m K for Ca-rich pyrope–almandines [11]. Indeed, a lower value of k_0 is to be expected for this series, as the compositional substitution involved is more complicated (three ionic species populate the octahedral sites as compared to two species in the other garnets). Thus, the calculated compositional dependence across the majorite–pyrope binary is consistent with available data on other garnets.

6. Parameterizations for geophysical modeling

6.1. Thermodynamic properties

Heat capacity is directly used in mantle convection models, whereas entropy indirectly pertains, as S constrains phase boundaries through Clapeyron's equation. Our calculations corroborate that the heat capacity of majorite measured from 150 to 700 K [37] was obtained from a disordered sample and thus is appropriate for extrapolation to mantle conditions. Above 700 K, C_P of pyrope [40] (given in Eq. 5) should be used, as all spectroscopic models of pyrope–majorite garnets converge at this temperature. Below 150 K, pyrope data [36] should be used as well. The total entropy of 266 J/mol K obtained for pure majorite represents a fully disordered octahedral site, as expected from twinning relations or symmetry analysis [31]. Although the $I4_1/acd$ structure was not considered in our calculations, this detail is immaterial, as both cubic and $I4_1/acd$ garnet have one octahedral site.

6.2. Inference of k_0 for mantle garnets

Garnet in the TZ may be ∼70% majorite [44]. A garnet composition on the pyrope–majorite binary with this Mj content has k_0 near 2.7 W/m K (Fig. 5 and Table 2). However, available mantle majorites include substantial amounts of other cations (e.g. Fe, Ca, Na, Cr and Ti), much like eclogitic garnets from the lithosphere [45]. From Giesting and Hofmeister [11], upper mantle (UM) garnets with 13% grossular component have k_0 that is 9% lower than samples without Ca but similar Fe/Mg ratios along the pyrope–almandine binary. From this comparison, replacement of roughly 20% of the Mg by Ca and Fe in Mj_{75} garnets would reduce k_0 by 15%, leading to 2.3 W/m K, as the most likely value for TZ garnet is 2.3 W/m K.

7. Implications for the mantle

At mantle temperatures, the blackbody curve has the same peak position as the main Fe^{2+}

band [46], which is similar in strength and position in the silicates and oxides [47], and thus radiative transfer is roughly the same for all mantle phases. Given the available data, all silicates have k_{lat} proportional to $1/T^{1/2}$ and have a similar pressure response of d[ln k_{lat}]/d$P = (1/3+4\gamma_{th})/K_T$ [5]. The second most abundant phase in the lower mantle (LM) is ferropericlase. The end-member, MgO, has a very high k_0 of 52 W/m K, but because k_{lat} of simple oxides is proportional to $1/T$ (summarized in [5]), the lattice contribution of (Mg,Fe)O becomes small relative to that of perovskite for the high temperatures of the LM. The importance of ferropericlase to heat transfer is further reduced since perovskite volumetrically dominates. Thus, k_0 values of the various silicates indicate the relative effectiveness in transporting heat among the various phases in the mantle layers.

Low-symmetry phases (olivine, enstatite, and diopside) thought to be volumetrically important in the UM have k_0 from 4.5 to 5.2 W/m K [10,41,48]. A comparable value of 4.7 W/m K exists for the perovskite polymorph of $MgSiO_3$ [5,49], which represents the LM. Ringwoodite, which is the other major phase in the TZ, has a much higher k_0 of 10 W/m K [10]. Estimates of the garnet component in the TZ range from 40 to 70% by volume, depending on the petrological model (e.g. [7,8,50,51]). Pyrolitic models suggest the TZ has ∼40% garnet and ∼60% ringwoodite. For this case, the average k_0 of 6.9 W/m K for the TZ is high relative to that of the UM. In contrast, for models with 70% garnet, the average k_0 of 4.6 W/m K for the TZ is less than nominal values for both the UM and LM. Large proportions of garnet as well as extensive chemical substitutions within the garnet thus impede heat transfer through the TZ, relative to both UM and LM.

The disparate k_0 values for the two mineral structures expected in the TZ and the crucial location of this zone above the clearly circulating LM suggest that Earth's thermal state and mantle dynamics depend largely on the proportion of garnet from 410 to 670 km depth. Like the LM [52], the TZ is also a two-phase region with respect to stiffness, having disparate bulk moduli

(see [5,8,15] and references therein) and thus disparate rheologic behavior. These zones differ significantly because in the LM, the stiffer phase (perovskite) is also the better heat conductor (at mantle conditions) and clearly dominates volumetrically (> 80%), whereas for the TZ, the stiffer of the two phases (garnet) is the poorer heat conductor, and probably dominates volumetrically. Quantifying heat transfer in the mantle requires geodynamic modeling. However, aspects of the process are suggested from the association of low thermal conductivity with high garnet content in the TZ.

7.1. Are TZ temperatures sub-adiabatic?

The steep velocity profiles found in the TZ cannot be explained by adiabatic gradients for the phases possibly stable in this region [53]. Sinogeikin and Bass [53] modeled the velocity gradient with a gradual transformation of pyroxenes to majoritic garnets as depth increases. Such compositional models are underconstrained, suggesting that alternative proposals merit discussion in view of the heat transport within the layers.

The steep velocity profiles could be due to a chemical discontinuity between an essentially perovskite-structured (pyroxene stoichiometry) LM and an olivine-rich UM (pyrolite). For this scenario, the velocity profile in the TZ represents a gradual chemical change and adiabatic temperatures. If this is the case, then the progressive increase of olivine polymorphs towards the surface enhances the efficiency of heat transfer in the outer layers of the Earth.

If, instead, the composition of the mantle is more or less uniform (pyrolitic as is assumed for the UM), then the high thermal conductivity due to spinel-dominating garnet may allow the TZ to be a boundary layer between the UM and LM. However, the steeper conductive temperature gradient implied for such a boundary layer would suggest a shallow velocity profile for the TZ in an isochemical system, which is incompatible with seismic evidence. Therefore, assumption of a chemically homogeneous mantle is problematic.

The observed velocity profiles are compatible with a sub-adiabatic gradient. This in turn is compatible with a higher garnet content and thus an impeded heat flow. Possibly, the formation of the crust has siphoned off the radioactive isotopes, leaving the TZ barren, but not cold, as it is warmed by the LM expelling its own heat and that of the underlying core. Addressing the steep velocity gradients in view of the thermal properties of TZ phases points to a chemically layered mantle. The chemical layering may be as subtle as an increase in Ca, suggested by Sinogeikin and Bass [53], or it may be more pervasive.

7.2. A mechanism for mantle avalanche?

Intermittent, catastrophic overturns of a partially layered mantle system have been found in many approaches to numerical modeling of Earth's convection system, and have recently been tied with the length-of-day perturbation in the Cretaceous [54]. The exothermic phase boundary at 670 km and the change in viscosity with pressure, temperature, and phase, all of which are time-dependent, play key roles in the process leading to an avalanche [55]. The variable nature of mantle rheology has long been considered a prime driving force in thermal evolution (see [56]). However, thermal conductivity plays an undeniably important role in the temperature equation, which largely governs the time dependence of mantle convection (e.g. [3]). With this concept in mind, a thermally sluggish TZ could be the precursor to a mantle avalanche. We speculate that the process could operate as follows:

Low thermal conductivity in the TZ retains heat, and therefore contributes to the buoyancy of this layer relative to the surroundings, and is destabilizing. The relative warmth concomitantly decreases the viscosity, exacerbating the problem. Higher temperatures also promote the formation of garnet relative to phases with ilmenite or spinel structures. These later phases with few atoms in the unit cell have much higher thermal conductivity than does garnet. Mantle avalanches are thus hypothesized to result from positive feedback, which causes the TZ to become relatively buoyant compared to the cold, stiff UM with time.

Acknowledgements

References

[1] G. Schubert, D.L. Turcotte, P. Olson, Mantle Convection in the Earth and Planets, Cambridge University Press, Cambridge, 2001.

[2] F. Dubuffet, D.A. Yuen, M. Rabinowicz, Effects of a realistic mantle thermal conductivity on the patterns of 3-D convection, Earth Planet. Sci. Lett. 171 (1999) 401–409.

[3] D.A. Yuen, A.P. Vincent, S.Y. Bergeron, F. Dubuffet, A.A. Ten, V.C. Steinbach, L. Starin, Crossing of scales and nonlinearities in geophysical processes, in: E. Boschi et al. (Eds.), Problems in Geophysics for the New Millenium, Editrice Compositori, Bologna, 2000, pp. 405–465.

[4] A.P. Van den Berg, D.A. Yuen, V. Steinbach, The effects of variable thermal conductivity on mantle heat-transfer, Geophys. Res. Lett. 280 (2001) 875–878.

[5] A.M. Hofmeister, Mantle values of thermal conductivity and the geotherm from photon lifetimes, Science 283 (1999) 1699–1706.

[6] R.G. Ross, P. Andersson, B. Sundqvist, G. Bäckström, Thermal conductivity of solids and liquids under pressure, Rep. Prog. Phys. 47 (1984) 1347–1402.

[7] P. Vacher, A. Moquet, C. Sotin, Computation of seismic profiles from mineral physics; the importance of the non-olivine components for explaining the 660 km depth discontinuity, Phys. Earth Planet. Inter. 106 (1998) 275–298.

[8] D.J. Weidner, Y. Wang, Phase transformations; implications for mantle structure, in: Earth's Deep Interior; Mineral Physics and Tomography from the Atomic to the Global Scale, Geophysical Monograph 117, 2000, pp. 215–235.

[9] P.G. Silver, R.W. Carlson, P. Olson, Deep slabs, geochemical heterogeneity, and the large-scale structure of mantle convection: investigation of an enduring paradox, Annu. Rev. Earth Planet. Sci. 16 (1988) 477–541.

[10] A.M. Hofmeister, Thermal conductivity of spinels and olivines from vibrational spectroscopy: ambient conditions, Am. Mineral. 86 (2001) 1188–1208.

[11] P.A. Giesting, A.M. Hofmeister, Thermal conductivity of disordered garnets from infrared spectroscopy, Phys. Rev. B 65 (2002) paper #144305 (15 pp.).

[12] S.W. Kieffer, Thermodynamics and lattice vibrations of minerals: 3. Lattice dynamics and an approximation for minerals with application to simple substances and framework silicates, Rev. Geophys. Space Phys. 17 (1979) 35–59.

[13] A.M. Hofmeister, A. Chopelas, Thermodynamic properties of pyrope and grossular from vibrational spectroscopy, Am. Mineral. 76 (1991) 880–891.

[14] G.D. Gwanmesia, R.C. Liebermann, F. Guyot, Hot-pressing and characterization of polycrystals of β-Mg_2SiO_4 for acoustic velocity measurements, Geophys. Res. Lett. 17 (1990) 1331–1334.

[15] G.D. Gwanmesia, J. Liu, G. Chen, S. Kesson, S.M. Rigden, R.C. Liebermann, Elasticity of the pyrope ($Mg_3Al_2Si_3O_{12}$) - majorite ($Mg_4Si_4O_{12}$) garnets solid solution, Phys. Chem. Miner. 27 (2000) 445–452.

[16] B.L. Jolliff, R.L. Korotev, K.M. Rockow, Geochemistry and petrology of lunar meteorite Queen Alexandra Range 94281, a mixed mare and highland regolith breccia, with special emphasis on very-low-titanium mafic components, Meteor. Planet. Sci. 33 (1998) 581–601.

[17] A.M. Hofmeister, H.K. Mao, Evaluation of shear moduli and other properties of silicates with the spinel structure from IR spectroscopy, Am. Mineral. 86 (2001) 622–639.

[18] A.M. Hofmeister, P.A. Giesting, B. Wopenka, G.D. Gwanmesia, B.L. Jolliff, Vibrational spectroscopy of pyrope-majorite garnets: structure and order, Am. Mineral., in press.

[19] P.A. Giesting, Spectroscopy and Thermal Conductivity of Mantle Garnets, M.A. Thesis, Washington University, St. Louis, MO, 2002.

[20] P.A. Giesting, B. Wopenka, B.L. Jolliff, G.D. Gwanmesia, A.M. Hofmeister, H and C impurities in synthetic majorite garnets: implications for speciation and solubility, EOS Trans. Am. Geophys. Union 84 (2003) Fall Meet. V22B-0590.

[21] T. Kato, M. Kumazawa, Garnet phase of $MgSiO_3$ filling the pyroxene-ilmenite gap at very high temperature, Nature 316 (1985) 803–805.

[22] P. McMillan, M. Akaogi, E. Ohtani, Q. Williams, R. Nieman, R. Sato, Cation disorder in garnets along the $Mg_3Al_2Si_3O_{12}$-$Mg_4Si_4O_{12}$ join: an infrared, Raman, and NMR study, Phys. Chem. Miner. 16 (1989) 428–435.

[23] A.M. Hofmeister, T.J. Fagan, K.M. Campbell, R.B. Schaal, Single-crystal IR spectroscopy of pyrope-almandines with minor amounts of Mn and Ca, Am. Mineral. 81 (1996) 418–428.

[24] M.H. Manghnani, V. Vijayakumar, J.D. Bass, High-pressure Raman scattering study of majorite-garnet solid solutions in the system $Mg_4Si_4O_{12}$-$Mg_3Al_2Si_3O_{12}$, in: M.H. Manghnani et al. (Eds.), Properties of Earth and Planetary Materials at High Pressure and Temperature, AGU, Washington DC, 1998, pp. 129–137.

[25] M. Rauch, H. Keppler, W. Häfner, B. Poe, A. Wokaun,

A pressure-induced transition in $MgSiO_3$-rich garnet revealed by Raman spectroscopy, Am. Mineral. 81 (1996) 1289–1292.

[26] B.L. Phillips, D.A. Howell, R.J. Kirkpatrick, T. Gasparik, Investigaton of cation order in $MgSiO_3$-rich garnet using ^{29}Si and ^{27}Al MAS NMR spectroscopy, Am. Mineral. 77 (1992) 704–712.

[27] A. Nakatsuka, A. Yoshiasa, T. Yamanaka, O. Ohtaka, T. Katsura, E. Ito, Symmetry change of majorite solid-solution in the system $Mg_3Al_2Si_3O_{12}$-$MgSiO_3$, Am. Mineral. 94 (1999) 1135–1143.

[28] S. Heinemann, T.G. Sharp, F. Seifert, D.C. Rubie, The cubic-tetragonal phase transition in the system majorite $(Mg_4Si_4O_{12})$ - pyrope $(Mg_3Al_2Si_3O_{12})$, Phys. Chem. Miner. 24 (1997) 206–221.

[29] I.F. Chang, S.S. Mitra, Application of a modified long-range iso-displacement model to long-wavelength optic phonons of mixed crystals, Phys. Rev. 172 (1996) 924–933.

[30] R.J. Angel, L.W. Finger, R.M. Hazen, M. Kanzaki, D.J. Weidner, R.C. Liebermann, D.R. Veblen, Structure and twinning of single-crystal $MgSiO_3$ garnet synthesized at 17 GPa and 1800°C, Am. Mineral. 74 (1989) 509–512.

[31] D.M. Hatch, S. Ghose, Symmetry analysis of the phase transition and twinning in $MgSiO_3$ garnet: implications to mantle mineralogy, Am. Mineral. 74 (1989) 1221–1224.

[32] H.H. Ulbrich, D.R. Waldbaum, Structural and other contributions to the third-law entropies of silicates, Geochim. Cosmochim. Acta 40 (1976) 1–24.

[33] P. Gillet, P. Richet, F. Guyot, G. Fiquet, High-temperature thermodynamic properties of forsterite, J. Geophys. Res. 96 (1991) 11805–11816.

[34] D.C. Wallace, Thermodynamics of Crystals, Wiley, New York, 1972, sections 16 and 20.

[35] B.A. Kolesov, C.A. Geiger, Low-temperature single-crystal Raman spectrum of pyrope, Phys. Chem. Miner. 27 (2000) 645–649.

[36] H.T. Haselton, E.F. Westrum, Low-temperature heat capacities of synthetic pyrope, grossular, and $pyrope_{60}$-$grossular_{40}$, Geochim. Cosmochim. Acta 44 (1980) 701–709.

[37] H. Yusa, M. Akaogi, E. Ito, Calorimetric study of $MgSiO_3$ garnet and pyroxene: heat capacities, transition enthalpies, and equilibrium phase relations in $MgSiO_3$ at high pressures and temperatures, J. Geophys. Res. 98 (1993) 6453–6460.

[38] K.M. Krupka, B.S. Hemingway, R.A. Robie, D.M. Kerrick, High-temperature heat capacities and derived thermodynamic properties of anthophyllite, diopside, dolomite, enstatite, bronzite, talc, tremolite and wollastonite, Am. Mineral. 70 (1985) 261–271.

[39] N. Bolfan-Casanova, H. Keppler, D.C. Rubie, Water partitioning between nominally anhydrous minerals in the MgO-SiO_2-H_2O system up to 24 GPa: implications for the distribution of water in the Earth's mantle, Earth Planet. Sci. Lett. 182 (2000) 209–221.

[40] C. Tequi, R.A. Robie, B.S. Hemingway, D. Neuville, P. Richet, Thermodynamic and melting properties of pyrope, Geochim. Cosmochim. Acta 55 (1991) 1005–1010.

[41] M. Chai, J.M. Brown, L.J. Slutsky, Thermal diffusivity of mantle minerals, Phys. Chem. Miner. 23 (1996) 470–475.

[42] W.G. Spitzer, R.C. Miller, D.A. Kleinman, L.W. Howarth, Far-infrared dielectric dispersion in $BaTiO_3$, $SrTiO_3$, and TiO_2, Phys. Rev. 126 (1962) 1710–1721.

[43] F.D. Patel, E.C. Honea, I. Speth, S.A. Payne, R. Hutcheson, R. Equall, Laser demonstration of $Yb_3Al_5O_{12}$ (YbAG) and materials properties of highly doped Yb:YAG, IEEE J. Quantum Electron. 37 (2001) 135.

[44] Y. Nishihara, E. Takahashi, Phase relation and physical properties of an Al-depleted komatiite to 23 GPa, Earth Planet. Sci. Lett. 190 (2001) 65–77.

[45] T. Stachel, Diamonds from the asthenosphere and the transition zone, Eur. J. Miner. 13 (2001) 883–892.

[46] T.J. Shankland, U. Nitsan, A.G. Duba, Optical absorption and radiative heat transport in olivine at high temperature, J. Geophys. Res. 84 (1979) 1603–1610.

[47] N.L. Ross, Optical absorption spectra of transition zone minerals and implications for radiative heat transfer, Phys. Chem. Earth 22 (1997) 113–118.

[48] K. Horai, Thermal conductivity of rock-forming minerals, J. Geophys. Res. 76 (1971) 1278–1308.

[49] M. Osako, E. Ito, Thermal diffusivity of $MgSiO_3$ perovskite, Geophys. Res. Lett. 18 (2001) 239.

[50] J.D. Bass, D.L. Anderson, Composition of the upper mantle: geophysical test of two petrological models, Geophys. Res. Lett. 11 (1984) 229–232.

[51] K. Hirose, T. Yagi, K.I. Funakoshi, Y. Fei, S. Ono, In situ measurements of the phase transition boundary in $Mg_3Al_2Si_3O_{12}$, Earth Planet. Sci. Lett. 184 (2001) 567–573.

[52] D. Yamazaki, S.-I. Karato, Some mineral physics constraints on the rheology and geothermal structure of Earth's lower mantle, Am. Mineral. 86 (2001) 385–391.

[53] S.V. Sinogeikin, J.D. Bass, Elasticity of majorite and a majorite-pyrope solid solution to high pressure: implications for the transition zone, Geophys. Res. Lett. 29 (2002) 10.1029/2001GL013937 (4 pp).

[54] P. Machetel, E. Thomassot, Cretaceous length of day perturbation by mantle avalanche, Earth Planet. Sci. Lett. 202 (2002) 379–386.

[55] D. Brunet, P. Machetel, Large-scale tectonic features induced by mantle avalanches with phase, temperature, and pressure lateral variations of viscosity, J. Geophys. Res. 103 (1998) 4929–4945.

[56] D. Tozer, Heat transfer and convection currents, Philos. Trans. R. Soc. London A 258 (1965) 252–271.